A type 2C protein phosphatase activates high-affinity nitrate uptake by dephosphorylating NRT2.1

Yuri Ohkubo[1], Keiko Kuwata[2] and Yoshikatsu Matsubayashi[1]*

[1]Division of Biological Science, Graduate School of Science, Nagoya University

[2]Institute of Transformative Bio-Molecules, Nagoya University

Chikusa, Nagoya 464-8602, Japan

*Correspondence to: Y. Matsubayashi (matsu@bio.nagoya-u.ac.jp)

Nitrate transporter NRT2.1, which plays a central role in high-affinity nitrate uptake in roots, is activated at the post-translational level in response to nitrogen (N) starvation [1, 2]. However, critical enzymes required for post-translational activation of NRT2.1 remain to be identified. Here, we show that a type 2C protein phosphatase, designated CEPD-induced phosphatase (CEPH), activates high-affinity nitrate uptake by directly dephosphorylating S^{501} of NRT2.1, a residue that functions as a negative phospho-switch [2]. *CEPH* is predominantly expressed in epidermal and cortex cells in roots and up-regulated by N starvation via a CEPDL2/CEPD1/2-mediated long-distance signaling from shoots [3, 4]. Loss of *CEPH* leads to a marked decrease in high-affinity nitrate uptake, tissue nitrate content, and plant biomass. Collectively, our results identify CEPH as a crucial enzyme in N starvation-dependent activation of NRT2.1, providing molecular and mechanistic insights into how plants regulate high-affinity nitrate uptake at the post-translational level in response to the N environment.

Nitrate (NO_3^-) uptake and assimilation are a critical process for plant growth and development. To adapt to natural fluctuations in environmental nitrogen (N), plants have evolved two types of nitrate uptake systems: a high-affinity transport system (HATS) for low external nitrate concentrations, and a low-affinity transport system (LATS) for high external nitrate concentrations [5]. In *Arabidopsis*, the HATS is composed of NRT2 family proteins [6-8], including NRT2.1, NRT2.2, and NRT2.4, whereas the LATS is mediated by NRT1 family proteins [9, 10], such as NRT1.1 and NRT1.2. NRT1.1 is also known as a dual-affinity

transporter, which can facilitate nitrate uptake over a wide range of nitrate concentrations [11]. In natural field environments, where nitrate is often limiting, the HATS accounts for the majority of root nitrate uptake activity [12]. NRT2.1 plays a particularly predominant role in high-affinity nitrate uptake in the root, as *nrt2.1* mutants exhibit up to 75% loss of HATS activity [7, 13].

Expression of NRT2.1 is regulated primarily at the transcriptional level in response to changes in both the external N environment and the N demand of the whole plant [14, 15]. However, evidence accumulated over the past 20 years suggests that NRT2.1 activity is also tightly regulated at the post-translational level [1, 16-18]. Global phosphoproteomics profiling of *Arabidopsis* membrane fractions revealed that NRT2.1 is phosphorylated at multiple sites, including S^{11}, S^{21}, S^{28}, S^{501} and T^{521}, with the phosphorylation pattern differing depending on the N environment [2, 19, 20]. Phosphorylation of S^{21} tends to increase under nitrate-replete conditions [20]. Conversely, phosphorylation of S^{28} is induced by nitrate limitation [19, 21]. The results of recent residue-substitution experiments suggest that phosphorylation of S^{28} within the N-terminal tail is important for protein stabilization of NRT2.1 in response to N limitation [21]. By contrast, S^{501}, located within the C-terminal tail of NRT2.1, is phosphorylated under high-nitrate conditions [2]. Importantly, substitution of S^{501} with Asp, which mimics the phosphorylated state, leads to complete inactivation of NRT2.1 without modulation of the protein's stability or its interaction with NRT3.1 [2]. As substitution of S^{501} with Ala conversely results in constitutive activation of NRT2.1, one attractive interpretation is that phosphorylation of S^{501} functions as a negative phospho-switch that regulates NRT2.1 activity depending on the N environment. However, the key enzymes required for this dephosphorylation-dependent activation of NRT2.1 remain to be identified.

Plants employ long-distance peptide signaling to maintain N homeostasis, especially when faced with low availability in soil and/or high N demand in the shoots. When roots are subjected to nitrate-limited conditions, the starvation-induced peptide CEP acts as a root-derived ascending N-starvation signal to the shoots, where its perception by receptors leads to the production of shoot-derived descending CEPD1 (CEP downstream 1) and CEPD2, which upregulate expression of nitrate transporter genes in the roots [3, 22, 23]. In parallel with this system, when root N uptake is insufficient to meet the N demand of the shoots, CEPDL2 expression is induced in shoots, and this protein acts as a descending signal that elevates high-affinity nitrate uptake in the roots [4]. Loss of both the CEPDL2 and CEPD1/2 pathways was shown to result in a marked decrease in high-affinity nitrate uptake by the roots, thereby

highlighting the critical role of these long-distance mobile peptides in N homeostasis in plants. The evidence currently available thus suggests that the primary function of the CEPDL2/CEPD1/2 pathway is to regulate transcription of high-affinity nitrate transporter genes in the roots. However, a number of genes associated with CEPDL2/CEPD1/2 signaling remain to be analyzed.

During the course of characterizing CEPDL2 function using an overexpression approach, we found that expression of a PP2C family phosphatase, At4g32950, is highly up-regulated in roots by CEPDL2 even under N-replete conditions (10 mM NH_4^+, 10 mM NO_3^-) (Fig. 1a, Supplementary Table 1). The abundance ratio of *At4g32950* transcripts in *CEPDL2*-overexpressing plants (*CEPDL2ox*) compared to that of wild-type (WT) plants was comparable to that of *NRT2.1*, one of the major targets of the CEPDL2 signaling pathway. At4g32950 belongs to the PP2C subfamily E, which consists of 12 members in *Arabidopsis* [24, 25], but none of the other members of this family showed a response to CEPDL2 (Fig. 1a). At4g32950 has close homologues in other plant species, both dicots such as potato [26] and *Medicago truncatula* [27] and monocots such as rice [28] and maize [29], but not in the moss *Physcomitrella patens* [30] (Extended Data Fig. 1a). *At4g32950* expression also increased following overexpression of CEPD1 or CEPD2, both of which are shoot-to-root mobile signals involved in systemic N-demand signaling.

We also found that *At4g32950* expression is greatly affected by the composition and concentration of N in the culture medium. When plants were grown in medium containing 10 mM NO_3^- as the sole N source (devoid of NH_4^+), basal expression of *At4g32950* was elevated 11.4-fold compared with plants grown under N-replete conditions, demonstrating that NH_4^+ negatively regulates *At4g32950* expression (Fig. 1b). Overexpression of *CEPDL2* under 10 mM NO_3^- condition further increased *At4g32950* expression by 4.7-fold.

When the medium NO_3^- concentration was reduced to 3, 1, or 0.3 mM, basal expression of *At4g32950* markedly increased (Fig. 1c). Importantly, N starvation-dependent up-regulation of *At4g32950* was almost abolished in the *cepd1,2 cepdl2* triple mutant (Fig. 1c, Extended Data Fig. 1b). The contribution of CEPDL2/CEPD1/2 toward *At4g32950* induction under 1 mM or 0.3 mM NO_3^- conditions was even more prominent than that toward *NRT2.1* induction (Fig. 1c, Extended Data Fig. 1c). In contrast, the *cepd1,2* double mutant and *cepdl2* single mutant showed no changes in *At4g32950* expression level (Fig. 1d). These results indicate that expression of *At4g32950* in roots is positively regulated by N starvation via the redundant CEPDL2 and CEPD1/2 pathways from the shoots.

Analysis of transgenic *Arabidopsis* lines expressing *At4g32950* promoter–β-glucuronidase (GUS) constructs revealed that the *At4g32950* promoter is preferentially active in the roots (Fig. 1e). In cross sections, *At4g32950* promoter activity was strongest in epidermal and cortical cells, but faint activity extended over the endodermal and pericycle cell layers (Fig. 1f). At4g32950-GFP, which was determined to be functional by complementation analyses (described below), localized in the cytosol in the roots (Fig. 1g). These results indicate that a root-specific PP2C family phosphatase, At4g32950, is a downstream target of CEPDL2/CEPD1/2 signaling, which is required for systemic regulation of N homeostasis. Accordingly, we designated this protein phosphatase CEPH (CEPD-induced phosphatase).

To elucidate the function of CEPH, we isolated mutants carrying a T-DNA insertion in *CEPH*, which we designated *ceph-1* (Fig. 2a). The insertion site and absence of full-length transcripts for this gene were confirmed by genomic PCR and RT-PCR analyses (Fig. 2b). When plants were grown under 1 mM NO_3^- conditions in which expression of *CEPH* is up-regulated, the *ceph-1* mutant exhibited a substantially smaller rosette with slightly yellowish leaves, which weighed 60% of the leaves of WT plants (Fig. 2c, 2d). This phenotype was fully complemented by transformation with the *CEPH* or *CEPH-GFP* genes (Fig. 2c–f, Extended Data Fig. 2a–b). Root fresh weight was also lower in the *ceph-1* mutant (Fig. 2d), but primary root length was not altered (Extended Data Fig. 2c–d). The lateral root of the *ceph-1* mutant was slightly longer than that of WT plants (Extended Data Fig. 2e). Under N-replete conditions (10 mM NH_4^+, 10 mM NO_3^-) in which *CEPH* expression is repressed, the *ceph-1* mutant exhibited no obvious phenotypes (Extended Data Fig. 2f–g).

The nitrate content of the shoots and roots of *ceph-1* plants decreased to 37% and 56%, respectively, of that of WT plants, suggesting that CEPH functions in a pathway regulating N acquisition (Fig. 2e). Accordingly, we measured root nitrate influx in *ceph-1* plants at 0.2 and 10 mM external concentrations of $^{15}NO_3^-$ to discriminate between the activities of the high- and low-affinity nitrate transport systems (i.e., HATS and LATS, respectively). When incubated in 0.2 mM $^{15}NO_3^-$, *ceph-1* plants that had been cultured in 1 mM NO_3^- for 14 d exhibited only 62% of the $^{15}NO_3^-$ high-affinity uptake activity of WT plants (Fig. 2f). In contrast, when LATS activity was calculated as the difference between root $^{15}NO_3^-$ influx measured at 10 and 0.2 mM, only a marginal difference was observed between WT and *ceph-1* plants (Extended Data Fig. 2h). However, the *ceph-1* mutation did not affect the transcription of genes involved in nitrate uptake, such as *NRT2.1*, *NRT2.2*,

NRT2.4, *NRT3.1* and *NRT1.1* (Extended Data Fig. 2i). Instead, expression of *CEPDL2* was increased in the shoot of *ceph-1* plants, most likely reflecting changes in N status in the shoot (Extended Data Fig. 2j).

We further analyzed the HATS activity in the roots of transgenic plants expressing *CEPH* under control of an estradiol-inducible *XVE* system (*XVE-CEPH*). When 14-day-old plants grown on medium containing 10 mM NO_3^- were treated with estradiol for 6 h, HATS activity increased 25% compared with mock-treated plants (Fig. 2g, Extended Data Fig. 2k). These results indicate that CEPH regulates high-affinity nitrate uptake in the roots possibly at the posttranslational level.

Because CEPH is a protein phosphatase, we hypothesized that its substrate protein is involved in high-affinity nitrate uptake and that phosphorylation of the substrate protein would be increased in the roots of *ceph-1* plants. To identify proteins differentially phosphorylated between *ceph-1* and WT plants, we employed unbiased quantitative phosphoproteomic profiling in which two samples, one grown under conditions of the naturally occurring ^{14}N environment and the other metabolically labeled with stable isotope ^{15}N, were compared using mass spectrometry [31].

WT and *ceph-1* plants were cultured on medium containing $^{14}NO_3^-$ or $^{15}NO_3^-$ for 14 d in a reciprocal manner for a biological duplicate (^{14}N WT/^{15}N *ceph-1* [forward experiment] and ^{15}N WT/^{14}N *ceph-1* [reciprocal experiment]). Root samples from ^{14}N-labeled and ^{15}N-labeled plants were collected and mixed, and total proteins were extracted from the samples and subjected to Lys-C or trypsin digestion. In the Lys-C–digested sample, phosphopeptide enrichment followed by mass spectrometric analyses allowed the identification of 1,448 $^{14}N/^{15}N$ phosphopeptide ion peak pairs (including charge state variants) (Extended Data Fig. 3a). The mass spectra of 8 phosphopeptides with a *ceph-1*/WT abundance ratio ≥1.5 were manually inspected. In a similar procedure, we identified 2,051 $^{14}N/^{15}N$ phosphopeptide ion peak pairs in the trypsin-digested sample (Extended Data Fig. 3b), among which 3 phosphopeptides exhibited a *ceph-1*/WT abundance ratio ≥1.5. Of the 11 phosphopeptide ion peaks manually inspected, two peaks from the Lys-C–digested sample were consistently more abundant in *ceph-1* in both the forward and reciprocal samples. These two peaks represented phosphopeptide ions originating from the high-affinity nitrate transporter NRT2.1.

The two phosphopeptide ion peaks derived from NRT2.1 corresponded to a single peptide, NMHQG[$S^{501}(PO_3H_2)$]LRFAENAK (Fig. 3a). The phosphorylation level of S^{501} of NRT2.1 increased by 2.2- and 3.1-fold in the *ceph-1* mutant in the forward and reciprocal experiments (Fig. 3b), respectively, whereas the abundance of NRT2.1 protein was comparable between WT and *ceph-1* plants, as indicated by the abundance of tryptic fragments of NRT2.1 analyzed without phosphopeptide enrichment (Extended Data Fig. 4a). Among known phosphorylation sites in NRT2.1, the elevated phosphorylation in *ceph-1* was specific to S^{501} and not observed at other sites, such as S^{28} and T^{521} (Fig. 3c, Extended Data Fig. 4b). Importantly, S^{501} phosphorylation has been shown to act as a negative phospho-switch that represses NRT2.1 activity [2]. We confirmed under our experimental conditions that substitution of S^{501} of NRT2.1 with Asp (NRT2.1[S501D]), which mimics the phosphorylated state, led to complete inactivation of NRT2.1 (Extended Data Fig. 5a–d). Intriguingly, transformation of *ceph-1* plants with an *NRT2.1[S501A]* construct, which expresses the NRT2.1 variant mimicking the dephosphorylated active state, rescued the nitrate uptake activity to a level comparable with that of the control plants expressing NRT2.1[S501A] (Extended Data Fig. 5e). Thus, the observed *ceph-1* phenotype characterized by decreased nitrate uptake and tissue nitrate content can be explained by the down-regulation of NRT2.1 activity due to enhanced phosphorylation of S^{501}.

To test whether CEPH directly dephosphorylates NRT2.1 at S^{501}, a synthetic 15-residue phosphopeptide corresponding to the sequence surrounding S^{501} of NRT2.1 was incubated with immuno-purified CEPH-GFP expressed in *Arabidopsis*. LC-MS analyses of the reaction products showed that S^{501} of the NRT2.1 peptide fragment was dephosphorylated by CEPH-GFP, indicating that S^{501} of the NRT2.1 is a direct target of CEPH (Fig. 3d). Assays using a control phosphopeptide corresponding to the sequence surrounding S^{28} of NRT2.1 yielded no dephosphorylated peptides, indicating that CEPH phosphatase activity against NRT2.1 is highly specific for S^{501} (Extended Data Fig. 4c).

We further analyzed the phosphorylation level of S^{501} of NRT2.1 in the roots of transgenic plants carrying the estradiol-inducible *XVE-CEPH* system. When transgenic plants grown on medium containing 10 mM NO_3^- were treated with estradiol for 6 h, the phosphorylation level of S^{501} of NRT2.1 decreased to 46% and 59% of that of mock-treated plants in the forward and reciprocal experiments, respectively, without alteration of protein expression levels (Fig. 3e, Extended Data Fig. 5f). We already showed (Fig. 2g) that estradiol treatment of these *XVE-CEPH* plants led to a 25% increase in HATS activity. Taken together,

our results demonstrate that CEPH activates high-affinity nitrate uptake via direct dephosphorylation of S^{501} of NRT2.1.

In this work, we identified a novel protein phosphatase, CEPH, which directly activates NRT2.1, thus revealing a new regulatory pathway of the high-affinity nitrate uptake system in plants. *Arabidopsis* expresses a large family of PP2C-type phosphatases consisting of 80 members, which can be further divided into 12 subfamilies, designated A-L [24, 25]. CEPH belongs to subfamily E, one of the least understood PP2C subfamilies in *Arabidopsis*. The *Arabidopsis* PP2C-E subfamily includes 12 members, of which *EGR1*, *EGR2* and *EGR3* are the only phenotypically characterized genes to date [32]. As PP2C function tends to be conserved within subfamilies, as exemplified by subfamilies A and B, in which individual members have emerged as regulators of ABA responses and MAPK signaling, respectively, our findings enhance understanding of the biological functions of PP2C subfamily E during plant growth and development.

Expression of *CEPH* in roots is regulated by the shoot-derived long distance signals, CEPDL2 and CEPD1/2, which mediate shoot N demand and local root N deficiency, respectively. When roots are subjected to nitrate-limited conditions and cannot take up sufficient nitrate to meet shoot N demand, both the CEPDL2 and CEPD1/2 pathways are highly up-regulated, leading to maximum expression of *CEPH*. Given that expression of the *NRT2.1* gene is controlled at the transcriptional level by shoot-derived signals, including CEPDL2 and CEPD1/2 [3, 4], our data indicate that systemic regulation of NRT2.1 activity is facilitated by the dual action of transcriptional control and post-translational switching.

Plants generally adapt to nutrient depletion in soil by up-regulating the expression of corresponding transporter proteins to increase nutrient acquisition capacity. However, this system suffers from an apparent paradox during N starvation, as the rate of *de novo* protein synthesis is restricted by the size of the free amino acid pool, which can be perturbed by N starvation. Phospho-switching, by contrast, requires only catalytic quantities of kinases and phosphatases to regulate the activity of target transporter proteins. It is thus plausible that plants express excess NRT2.1 protein under N-replete conditions and maintain a subset of NRT2.1 in the inactive phosphorylated form via the activity of an as yet uncharacterized protein kinase. Activation of the inactive phosphorylated NRT2.1 pool by phosphatase CEPH consumes less energy than *de novo* NRT2.1 protein synthesis. Indeed, under environmental conditions of very low nitrate concentrations, the CEPDL2 and CEPD1/2 pathways predominantly up-regulate *CEPH* rather than *NRT2.1*. CEPH is conserved in both dicots and

monocots. Plants thus employ this efficient 'up-front' strategy to adapt to, and survive in, fluctuating N environments.

Methods

Plant materials and growth conditions. The *cepdl2-1* single*, cepd1-1 cepd2-1* double, and *cepd1-1 cepd2-1 cepdl2-1* triple mutants (Nössen background) were described previously [3, 4]. The *ceph-1* mutant was obtained from the GABI-Kat *Arabidopsis* mutant collection (GABI_787G04, Columbia (Col) background) [33]. The *nrt2.1-2.2* double mutant was obtained from the SALK T-DNA mutant collection (SALK_035429, Col background). For complementation analysis, the full-length *CEPH* genomic fragment containing the 2.0-kb promoter region was cloned into the binary vector pCAMBIA1300-BASTA using an In-Fusion HD cloning kit (Clontech). The constructs were introduced into the *ceph-1* mutant by *Agrobacterium*-mediated transformation. For estradiol-inducible expression of *CEPH*, a cDNA of *CEPH* was obtained by RT-PCR using total RNA isolated from *Arabidopsis* roots. The resulting fragment was cloned into the *Xho*I/*Spe*I-digested estradiol-inducible binary vector pER8 [34] using an In-Fusion HD cloning kit. The constructs were introduced into wild-type Col. For estradiol-mediated *CEPH* expression, roots of 14-day-old transgenic plants expressing *CEPH* under control of the estradiol-inducible promoter were treated with β-estradiol for 6 h by direct addition of 2 ml of 50 μM β-estradiol solution onto the transgenic plants on the plates. For point mutation analysis of NRT2.1, the full-length *NRT2.1* genomic fragment containing the 1,335-bp promoter region was cloned into the binary vector pCAMBIA1300-BASTA using an In-Fusion HD cloning kit. NRT2.1 mutations were introduced by PCR with primers pairs containing the desired mutation. The constructs were introduced into the *nrt2.1-2.2* and *ceph-1* mutant. Transgenic plants overexpressing *CEPDL2* (*CEPDL2ox*), *CEPD1* (*CEPD1ox*) and *CEPD2* (*CEPD2ox*) were described previously (Col background) [3, 4]. *Arabidopsis* ecotype Col or Nössen plants were used as the WT depending on the experimental design. Surface-sterilized seeds were sown on B5 medium (1% sucrose) solidified using 1.5% agar in 13 × 10 cm plastic plates (18 seeds × 3 rows/plate) and grown vertically at 22°C with continuous light at an intensity of 80 $\mu mol \cdot m^{-2} \cdot s^{-1}$. After 7 d, seedlings were transferred to modified Murashige-Skoog medium solidified using 1.5% agar in 13 × 10 cm plastic plates (12 seedlings/plate) and further grown vertically at 22°C with

continuous light. Modified Murashige-Skoog medium for N-replete conditions contains 10 mM NH_4Cl and 10 mM KNO_3 as N and K sources, respectively, and half-strength concentrations of the other elements and 0.5% sucrose, adjusted to pH 5.7 with KOH. For 10 mM NO_3^- medium, 10 mM KNO_3 was added as the sole source of N and K. For 3 mM NO_3^- medium, 3 mM KNO_3 and 7 mM KCl were added. For 1 mM NO_3^- medium, 1 mM KNO_3 and 9 mM KCl were added. For 0.3 mM NO_3^- medium, 0.3 mM KNO_3 and 9.7 mM KCl were added. At least three independent biological replicates were performed for each experiment.

Microarray analysis. An RNeasy kit (Qiagen) was used to isolate total RNA from roots of WT (Col), *CEPD1ox*, *CEPD2ox* and *CEPDL2ox* plants grown on N-replete vertical plates for 14 d. Labeled complementary RNA was hybridized using an Affymetrix GeneChip *Arabidopsis* Gene 1.0 ST array according to the manufacturer's protocol.

Real-time RT-qPCR. Total RNA was isolated from the roots or shoots of plants grown under indicated conditions using an RNeasy kit. First-strand cDNA was synthesized from 2 μg of root-derived total RNA using the Superscript IV first-strand synthesis system (Invitrogen) according to the manufacturer's protocol. Primers and probes were designed using Probe Finder software from the Universal Probe Library assay design center (Roche Applied Science, Germany). Real-time RT-qPCR was performed using a StepOne system (Applied Biosystems). Constitutively expressed *EF-1α* was used as the reference gene for normalization of the RT-qPCR data. All statistical analyses were performed using GraphPad Prism software, version 8.

Promoter GUS analysis. For β-glucuronidase (GUS) reporter-aided analysis of *CEPH* promoter activity, we amplified the 2.0-kb upstream sequences of the predicted ATG start codons of each gene using genomic PCR and cloned the fragments into a promoter-less pBI101 vector upstream of the GUS reporter gene using the In-Fusion cloning system (Clontech). GUS activity was visualized using a standard protocol with X-Gluc as the substrate. For root sectioning, roots were fixed in FAA solution (3.7% formaldehyde, 5% acetic acid and 50% ethanol), dehydrated through a graded ethanol series, and embedded in Technovit 7100 resin (Heraeus Kulzer, Germany) following the manufacturer's protocol. Sections were cut at 4-μm thickness using a rotary microtome (Leica RM2235), counter-stained with 0.05% Nile red, mounted with Entellan (Merck), and observed under a standard light microscope (Olympus BX60).

CEPH-GFP expression. For analysis of CEPH-GFP expression, 2.0-kb upstream sequences from the predicted ATG start codon of *CEPH*, the GFP-coding region, and the *CEPH* ORF were ligated in-frame in this order into the *Hin*dIII-, *Bam*HI-digested binary vector pCAMBIA1300-BASTA by four-component ligation using the In-Fusion cloning system. The resulting *CEPH-GFP* construct was introduced into WT or *ceph-1* mutant plants (for complementation test). For root imaging, cell outlines were stained with 50 μg/ml propidium iodide for 2 min and observed under a confocal laser-scanning microscope (Olympus FV300) with helium-neon laser excitation at 543 nm. GFP images were collected with argon laser excitation at 488 nm. Plasmolysis was induced by applying 0.8 M mannitol for 20 min.

Nitrate content. The concentration of NO_3^- ions in tissues was determined using an ion chromatography system (Dionex Aquion, Thermo Fisher Scientific). Shoots or roots of 10-day-old plants were powdered in liquid nitrogen and mixed with 1 ml of water to extract nitrate. After centrifugation, the crude tissue extract was diluted 10-fold with water, and 25-μl aliquots were analyzed on a Dionex IonPac AS22 column (4 mm i.d. × 250 mm) over 15 min. The mobile phase eluent consisted of 4.5 mM Na_2CO_3 and 1.4 mM $NaHCO_3$, employed at a flow rate of 1.2 ml/min at 30°C, and separation was monitored using a conductivity detector equipped with a Dionex AERS 500 suppressor unit.

Root ^{15}N influx. Vertically grown 14-day-old plants were sequentially transferred to 0.1 mM $CaSO_4$ for 1 min and then to modified Murashige-Skoog medium containing 0.2 mM or 10 mM $^{15}NO_3^-$ as the N source for 10 min. At the end of ^{15}N labeling, the roots were washed for 1 min in 0.1 mM $CaSO_4$ and separated from the shoots. The roots were lyophilized *in vacuo* and analyzed for total N and ^{15}N content using elemental analysis–isotope ratio mass spectrometry (Flash EA1112-DELTA V PLUS ConFlo III system, Thermo Fisher Scientific).

Stable isotope metabolic labeling with ^{14}N or ^{15}N. For quantitative phosphoproteomic analyses, WT (Col) and *ceph-1* seedlings were reciprocally labeled with light (normal) ^{14}N or heavy ^{15}N via metabolic incorporation. We defined ^{14}N-labeled WT/^{15}N-labeled *ceph-1* pairs as forward labeling and ^{15}N WT/^{14}N *ceph-1* pairs as reciprocal labeling. Surface-sterilized WT and *ceph-1* seeds were sown on either ^{14}N- or ^{15}N-containing B5 medium (1% sucrose) solidified using 1.5% agar in 13 × 10 cm plastic plates (18 seeds × 3 row/plate) and then grown vertically at 22°C for 7 d with continuous light. In ^{15}N B5 medium, $K^{14}NO_3$ and $(^{14}NH_4)_2SO_4$ were substituted with heavy nitrogen salts, $K^{15}NO_3$ and $(^{15}NH_4)_2SO_4$, respectively. After 7 d, the seedlings were transferred to 1 mM NO_3^- medium (with either $K^{14}NO_3$ or $K^{15}NO_3$) solidified using 1.5% purified agar in 13 × 10 cm plastic plates (12

seedlings/plate) and further grown vertically at 22°C for 7 d with continuous light. For forward labeled samples, ^{14}N-labeled WT roots were combined at a 1:1 fresh weight ratio with ^{15}N-labeled *ceph-1* roots. Similarly, ^{15}N-labeled WT roots were combined at a 1:1 ratio with ^{14}N-labeled *ceph-1* roots for reciprocal labeling. The combined root tissues (0.5-1.0 g) were frozen in liquid nitrogen and ground to a fine powder using a Multi-beads shocker (Yasui Kikai Corp., Japan). Total protein was extracted by mixing 500 mg of ground tissue with 2.5 ml of extraction buffer (250 mM Tris-HCl [pH 7.6], 290 mM sucrose, 25 mM EDTA, 1 mM DTT, 1 mM PMSF, 100 μM 1,10-phenanthroline, and 1× PhosSTOP phosphatase inhibitors [Roche]), followed by brief sonication in an ultrasonic bath for 30 s. The homogenate was centrifuged for 15 min at 5,000 × *g* at 4°C, and then the supernatant was collected in a new tube. Proteins contained in the supernatant were purified using a methanol/chloroform precipitation protocol [35] and dried under vacuum for 10 min. The dried pellets were solubilized in digestion buffer (8 M urea, 250 mM ammonium bicarbonate, and 1× PhosSTOP phosphatase inhibitors) at a final protein concentration of 2.0 mg/ml. The protein concentration was determined using a Bradford protein assay kit.

Protein digestion and phosphopeptide enrichment. Proteins (0.5 mg/250 μl) were reduced with 25 mM tris(2-carboxyethyl)phosphine (TCEP) at 37°C for 15 min, alkylated using 25 mM iodoacetamide at 37°C for 30 min in the dark, both with gentle shaking (1,000 rpm) following the standard protocol. Proteins were digested with Lys-C (FUJIFILM Wako, Japan) at an enzyme-protein ratio of 1:100 at 37°C for 3 h. This Lys-C digest was divided into two equal aliquots, and one aliquot was diluted to a urea concentration of 2 M with 100 mM Tris-HCl (pH 8.5), followed by digestion with trypsin (Promega) at an enzyme-protein ratio of 1:100 at 37°C overnight. The digestion was stopped by adding 1/20 volume of 20% TFA, and then Lys-C–digested and Lys-C/trypsin–double digested peptides were desalted using a MonoSpin C18 spin column (GL Science) according to the manufacturer's instructions. Eluates were evaporated to dryness *in vacuo*, reconstituted in 200 μl of 80% acetonitrile (0.1% TFA), and subjected to phosphopeptide enrichment using Fe(III)-IMAC cartridges (5 μl) on a AssayMAP Bravo platform (Agilent) at a flow rate of 5 μl/min according to the manufacturer’s protocol. Phosphopeptides were successively eluted with 20 μl of 20% acetonitrile (1% TFA), 20 μl of 25% acetonitrile (5% ammonia), and 20 μl of 25% acetonitrile (5% pyrrolidine). The second and third eluents were combined and acidified with 40 μl of 20% TFA. These two samples were concentrated and desalted using GL-Tip SDB (GL Science) tips according to the manufacturer's instructions. Desalted samples were

dried and stored at −30°C until analysis. The first eluent and the second/third eluents were separately analyzed by LC-MS/MS.

LC-MS/MS data acquisition. Nano LC-MS/MS analysis was performed using a Dionex U3000 gradient pump (Thermo Fisher Scientific) connected to a Q Exactive hybrid quadrupole-orbitrap mass spectrometer (Thermo Fisher Scientific). Enriched phosphopeptides were dissolved in 20 µl of 2% acetonitrile (0.1% TFA) and centrifuged at 20,000 × *g* for 5 min at 25°C, and two 7.5-µl aliquots of the supernatant (for technical duplicates) were used for LC-MS/MS analysis. Samples were loaded onto a trap column (L-column ODS [300 µm I.D. × 5 mm], CERI, Japan) and washed with 2% acetonitrile (0.1% TFA). Peptides were subsequently eluted from the trap column and separated on a nano-HPLC capillary column (NTCC-360/100 [100 µm I.D. × 125 mm], Nikkyo Technos, Japan) with a gradient of 5–40% acetonitrile (containing 0.5% acetic acid) over 100 min at a flow rate of 500 nl/min. The Q Exactive mass spectrometer was operated in data-dependent acquisition mode with dynamic exclusion enabled (10 s). Survey full-scan MS spectra (mass range 350–1,800) were acquired at a resolution of 70,000 with the maximum injection time set at 60 ms. The 10 most-intense peptide ions in each survey scan with a charge state ≥2 were selected for MS/MS fragmentation. MS/MS scans were performed by higher-energy collisional dissociation with the normalized collision energy set to 27.

Quantification of ^{14}N/^{15}N paired phosphopeptides. The MS/MS raw files were processed and analyzed with Proteome Discoverer 2.3 (Thermo Fisher Scientific) using the SEQUEST HT algorithm, searching against the TAIR10 *Arabidopsis* protein database. Separate searches were conducted for ^{14}N- and ^{15}N-labeled peptides. For ^{14}N-labeled light peptides, the following search parameters were employed: peptide mass range 350–5,000 Da; enzyme specificity trypsin or LysC (depending on the samples), with up to two missed cleavages; precursor ion and peptide fragment mass tolerances ± 10 ppm and ± 0.02 Da, respectively; static modification carbamidomethyl (C); dynamic modifications phosphorylation (S, T, Y) and oxidation (M). For ^{15}N-labeled heavy peptides, the basic search parameters were identical to those used for ^{14}N peptides, with the following exceptions: static modification ^{15}N(1) (A, D, E, F, G, I, L, P, V [+0.997 Da]), ^{15}N(2) (K, N, Q, W [+1.994 Da]), ^{15}N(3) (H [+2.991 Da]), ^{15}N(4) (R [+3.988 Da]), ^{15}N(1) carbamidomethylation (C [+58.018 Da]); dynamic modifications ^{15}N(1) (M, S, T, Y [+0.997 Da]), ^{15}N(1) phosphorylation (S, T, Y [+80.963 Da]), and ^{15}N(1) oxidation (M [+16.992 Da]). Peptide validation was performed using the Percolator algorithm, and only high-confidence peptides were used for peptide

identification and quantification. The resulting dataset, which included information on annotated sequences, modifications, master protein accession, charge, *m*/*z*, retention time, and precursor abundance for each identified peptide, was imported into Microsoft Excel 2016. Using the filter function of Excel, peptides with no phosphorylated residue were excluded from the list. The resulting phosphopeptides were further divided into ^{14}N- and ^{15}N-labeled groups on the basis of the ^{15}N incorporation status to give two separate datasets. If the same peptide ion with the same charge state appeared multiple times within each dataset, the peptide ion with the highest abundance was selected as representative using the "sort" and "remove duplicate" commands. Subsequently, ^{14}N- and ^{15}N-peptide pairs with the same sequence, phosphorylation sites, and charge state were retrieved by cross-referencing the data in the two datasets using the VLOOKUP function. An abundance ratio was calculated by pairwise comparison (*ceph-1*/WT) for each phosphopeptide. When one of the counterparts was absent in the corresponding datasets, the abundance ratio was defined as 0 (or 100). The entries were sorted according to the *ceph-1*/WT ratio, and only entities exhibiting a fold-change >1.5 in both the forward and reciprocal experiments were subjected to manual inspection of the mass spectra.

Synthesis of phosphopeptides. Phosphopeptides corresponding to the 15-residue sequence surrounding S^{28} (SFAFSVQ[$S^{28}(PO_3H_2)$]PIVHTDK), S^{501} (QKNMHQG[$S^{501}(PO_3H_2)$]LRFAENA) and T^{521} (RRVRSAA[$T^{521}(PO_3H_2)$]PPENTPN) of NRT2.1 were synthesized by Fmoc solid-phase chemistry using an automated peptide synthesizer (Biotage Initiator+ Alstra) on TrtA-PEG resin. All peptides were purified by reverse-phase HPLC.

***In vitro* phosphatase assay.** Roots of 14-day-old transgenic plants expressing CEPH-GFP under control of the native promoter (≈500 mg) were frozen in liquid nitrogen and ground to a fine powder using a Multi-beads shocker. Total proteins were extracted by mixing 500 mg of ground tissue with 2.0 ml of extraction buffer (50 mM Tris-HCl, 150 mM NaCl, 1% Triton X-100, cOmplete Mini EDTA-free Protease Inhibitor Cocktail [Roche, 1 tablet per 10 ml]), followed by brief sonication in an ultrasonic bath for 5 s. After incubation on ice for 30 min, the homogenate was centrifuged for 15 min at 10,000 × *g* and 4°C, and then the supernatant was collected in a new tube. Anti-GFP antibody (ab290, Abcam) was crosslinked with magnetic Dynabeads Protein G (Invitrogen) at 0.5 μg/μl beads with bis(sulfosuccinimidyl)suberate following the manufacturer's instructions. The supernatant was then incubated with 100 μl of antibody-beads at 4°C for 2 h. After washing three times

with wash buffer (50 mM Tris-HCl, 150 mM NaCl, 0.1% Triton X-100) and phosphatase buffer (50 mM Tris-HCl [pH 7.0], 60 mM $MgCl_2$, 0.1 mM EGTA, and 0.1% β-mercaptoethanol), CEPH-GFP captured on the beads was directly subjected to the phosphatase assay. Standard assays were performed in 50 µl of reaction mixture containing 50 mM Tris-HCl (pH 7.0), 60 mM $MgCl_2$, 0.1 mM EGTA, 0.1% β-mercaptoethanol, 200 µM phosphopeptides, and 10 µl of CEPH-GFP beads. The reaction mixture was incubated in a 96-well plate for 3 h at 30°C with shaking at 800 rpm. Reactions were terminated by the addition of 1/10 volume of 1.0% formic acid. Aliquots of this reaction mixture (5 µl) were analyzed by LC-MS using electrospray ionization in the selected ion monitoring mode with a maximum inject time of 50 ms. The isolation width was set to 3.0 *m*/*z*. LC-MS analysis was performed using a semi-micro HPLC system connected to an LCQ Deca XP-plus ESI ion-trap mass spectrometer. Samples were analyzed by reverse-phase HPLC (Cadenza CD-C18 column [2.0 ×150 mm]) with a gradient of 0–50% acetonitrile containing 0.1% formic acid over 15 min at a flow rate of 100 µl/min.

References

1. Laugier, E., Bouguyon, E., Mauries, A., Tillard, P., Gojon, A. & Lejay, L. Regulation of high-affinity nitrate uptake in roots of *Arabidopsis* depends predominantly on posttranscriptional control of the NRT2.1/NAR2.1 transport system. *Plant Physiol* **158**, 1067-1078 (2012).
2. Jacquot, A., Chaput, V., Mauries, A., Li, Z., Tillard, P., Fizames, C., Bonillo, P., Bellegarde, F., Laugier, E., Santoni, V., Hem, S., Martin, A., Gojon, A., Schulze, W. & Lejay, L. NRT2.1 C-terminus phosphorylation prevents root high affinity nitrate uptake activity inArabidopsis thaliana. *New Phytol* **228**, 1038-1054 (2020).
3. Ohkubo, Y., Tanaka, M., Tabata, R., Ogawa-Ohnishi, M. & Matsubayashi, Y. Shoot-to-root mobile polypeptides involved in systemic regulation of nitrogen acquisition. *Nat Plants* **3**, 17029 (2017).
4. Ota, R., Ohkubo, Y., Yamashita, Y., Ogawa-Ohnishi, M. & Matsubayashi, Y. Shoot-to-root mobile CEPD-like 2 integrates shoot nitrogen status to systemically regulate nitrate uptake in *Arabidopsis*. *Nat Commun* **11**, 641 (2020).
5. Wang, Y.Y., Cheng, Y.H., Chen, K.E. & Tsay, Y.F. Nitrate transport, signaling, and use efficiency. *Annu Rev Plant Biol* **69**, 85-122 (2018).
6. Wang, R. & Crawford, N.M. Genetic identification of a gene involved in constitutive, high-affinity nitrate transport in higher plants. *Proc Natl Acad Sci U S A* **93**, 9297-9301 (1996).
7. Filleur, S., Dorbe, M.F., Cerezo, M., Orsel, M., Granier, F., Gojon, A. & Daniel-Vedele, F. An *Arabidopsis* T-DNA mutant affected in *Nrt2* genes is impaired in nitrate uptake. *FEBS Lett* **489**, 220-224 (2001).
8. Kiba, T., Feria-Bourrellier, A.B., Lafouge, F., Lezhneva, L., Boutet-Mercey, S., Orsel, M., Brehaut, V., Miller, A., Daniel-Vedele, F., Sakakibara, H. & Krapp, A. The *Arabidopsis* nitrate transporter NRT2.4 plays a double role in roots and shoots of nitrogen-starved plants. *Plant Cell* **24**, 245-258 (2012).
9. Tsay, Y.F., Schroeder, J.I., Feldmann, K.A. & Crawford, N.M. The herbicide sensitivity gene *CHL1* of *Arabidopsis* encodes a nitrate-inducible nitrate transporter. *Cell* **72**, 705-713 (1993).
10. Huang, N.C., Liu, K.H., Lo, H.J. & Tsay, Y.F. Cloning and functional characterization of an *Arabidopsis* nitrate transporter gene that encodes a constitutive component of low-affinity uptake. *Plant Cell* **11**, 1381-1392 (1999).
11. Liu, K.H., Huang, C.Y. & Tsay, Y.F. CHL1 is a dual-affinity nitrate transporter of arabidopsis involved in multiple phases of nitrate uptake. *Plant Cell* **11**, 865-874 (1999).
12. Malagoli, P., Lainé, P., Le Deunff, E., Rossato, L., Ney, B. & Ourry, A. Modeling nitrogen uptake in oilseed rape cv Capitol during a growth cycle using influx kinetics of root nitrate transport systems and field experimental data. *Plant Physiol* **134**, 388-400 (2004).
13. Cerezo, M., Tillard, P., Filleur, S., Munos, S., Daniel-Vedele, F. & Gojon, A. Major alterations of the regulation of root NO_3^- uptake are associated with the mutation of *Nrt2.1* and *Nrt2.2* genes in *Arabidopsis*. *Plant Physiol* **127**, 262-271 (2001).
14. Lejay, L., Tillard, P., Lepetit, M., Olive, F., Filleur, S., Daniel-Vedele, F. & Gojon, A. Molecular and functional regulation of two NO_3^- uptake systems by N- and C-status of *Arabidopsis* plants. *Plant J* **18**, 509-519 (1999).
15. Gansel, X., Munos, S., Tillard, P. & Gojon, A. Differential regulation of the NO_3^- and NH_4^+ transporter genes *AtNrt2.1* and *AtAmt1.1* in *Arabidopsis*: relation with long-distance and local controls by N status of the plant. *Plant J* **26**, 143-155 (2001).

16. Fraisier, V., Gojon, A., Tillard, P. & Daniel-Vedele, F. Constitutive expression of a putative high-affinity nitrate transporter in *Nicotiana plumbaginifolia*: evidence for post-transcriptional regulation by a reduced nitrogen source. *Plant J* **23**, 489-496 (2000).
17. Wirth, J., Chopin, F., Santoni, V., Viennois, G., Tillard, P., Krapp, A., Lejay, L., Daniel-Vedele, F. & Gojon, A. Regulation of root nitrate uptake at the NRT2.1 protein level in *Arabidopsis thaliana*. *J Biol Chem* **282**, 23541-23552 (2007).
18. Jacquot, A., Li, Z., Gojon, A., Schulze, W. & Lejay, L. Post-translational regulation of nitrogen transporters in plants and microorganisms. *J Exp Bot* **68**, 2567-2580 (2017).
19. Engelsberger, W.R. & Schulze, W.X. Nitrate and ammonium lead to distinct global dynamic phosphorylation patterns when resupplied to nitrogen-starved *Arabidopsis* seedlings. *Plant J* **69**, 978-995 (2012).
20. Menz, J., Li, Z., Schulze, W.X. & Ludewig, U. Early nitrogen-deprivation responses in *Arabidopsis* roots reveal distinct differences on transcriptome and (phospho-) proteome levels between nitrate and ammonium nutrition. *Plant J* **88**, 717-734 (2016).
21. Zou, X., Liu, M.Y., Wu, W.H. & Wang, Y. Phosphorylation at Ser28 stabilizes the *Arabidopsis* nitrate transporter NRT2.1 in response to nitrate limitation. *J Integr Plant Biol* (2019).
22. Ohyama, K., Ogawa, M. & Matsubayashi, Y. Identification of a biologically active, small, secreted peptide in *Arabidopsis* by *in silico* gene screening, followed by LC-MS-based structure analysis. *Plant Journal* **55**, 152-160 (2008).
23. Tabata, R., Sumida, K., Yoshii, T., Ohyama, K., Shinohara, H. & Matsubayashi, Y. Perception of root-derived peptides by shoot LRR-RKs mediates systemic N-demand signaling. *Science* **346**, 343-346 (2014).
24. Fuchs, S., Grill, E., Meskiene, I. & Schweighofer, A. Type 2C protein phosphatases in plants. *FEBS J* **280**, 681-693 (2013).
25. Bhaskara, G.B., Wong, M.M. & Verslues, P.E. The flip side of phospho-signalling: Regulation of protein dephosphorylation and the protein phosphatase 2Cs. *Plant Cell Environ* **42**, 2913-2930 (2019).
26. Wang, Y.F., Liao, Y.Q., Wang, Y.P., Yang, J.W., Zhang, N. & Si, H.J. Genome-wide identification and expression analysis of StPP2C gene family in response to multiple stresses in potato (Solarium tuberosum L.). *J Integr Agr* **19**, 1609-1624 (2020).
27. Yang, Q., Liu, K., Niu, X.C., Wang, Q., Wan, Y.Q., Yang, F.Y., Li, G.J., Wang, Y.F. & Wang, R.G. Genome-wide Identification of PP2C Genes and Their Expression Profiling in Response to Drought and Cold Stresses in Medicago truncatula. *Sci Rep-Uk* **8** (2018).
28. Xue, T.T., Wang, D., Zhang, S.Z., Ehlting, J., Ni, F., Jakab, S., Zheng, C.C. & Zhong, Y. Genome-wide and expression analysis of protein phosphatase 2C in rice and Arabidopsis. *Bmc Genomics* **9** (2008).
29. Fan, K., Yuan, S.N., Chen, J., Chen, Y.R., Li, Z.W., Lin, W.W., Zhang, Y.Q., Liu, J.P. & Lin, W.X. Molecular evolution and lineage-specific expansion of the PP2C family in Zea mays. *Planta* **250**, 1521-1538 (2019).
30. Komatsu, K., Nishikawa, Y., Ohtsuka, T., Taji, T., Quatrano, R.S., Tanaka, S. & Sakata, Y. Functional analyses of the ABI1-related protein phosphatase type 2C reveal evolutionarily conserved regulation of abscisic acid signaling between Arabidopsis and the moss Physcomitrella patens. *Plant Molecular Biology* **70**, 327-340 (2009).

31. Nelson, C.J., Huttlin, E.L., Hegeman, A.D., Harms, A.C. & Sussman, M.R. Implications of ^{15}N-metabolic labeling for automated peptide identification in *Arabidopsis thaliana*. *Proteomics* **7**, 1279-1292 (2007).
32. Bhaskara, G.B., Wen, T.N., Nguyen, T.T. & Verslues, P.E. Protein Phosphatase 2Cs and Microtubule-Associated Stress Protein 1 Control Microtubule Stability, Plant Growth, and Drought Response. *Plant Cell* **29**, 169-191 (2017).
33. Kleinboelting, N., Huep, G., Kloetgen, A., Viehoever, P. & Weisshaar, B. GABI-Kat SimpleSearch: new features of the *Arabidopsis thaliana* T-DNA mutant database. *Nucleic Acids Res* **40**, D1211-1215 (2012).
34. Zuo, J., Niu, Q.W. & Chua, N.H. Technical advance: An estrogen receptor-based transactivator XVE mediates highly inducible gene expression in transgenic plants. *Plant J* **24**, 265-273 (2000).
35. Wessel, D. & Flugge, U.I. A method for the quantitative recovery of protein in dilute solution in the presence of detergents and lipids. *Anal Biochem* **138**, 141-143 (1984).

Data Availability Statement

The data that support the findings of this study are available from the corresponding author upon request. The microarray data have been deposited in the NCBI Gene Expression Omnibus (GEO) under accession number GSE160649. The raw mass spectrometry data have been deposited in the ProteomeXchange Consortium via PRIDE partner repository under accession number PXD022343.

Acknowledgments

We thank Hiroyuki Fukuda (Agilent Technologies) for technical advice regarding phosphopeptide enrichment. This research was supported by a Grant-in-Aid for Scientific Research (S) (No. 18H05274 to Y.M.), Grant-in-Aid for Transformative Research Areas (A) (No. 20H05907 to Y.M.) and a Grant-in-Aid for JSPS Fellows (No. 20J20049 to Y.O.) from the Japan Society for the Promotion of Science.

Author Contributions

Y.M. and Y.O. conceived this project and designed the experiments. Y.O. performed all of the biological experiments. K.K. performed phosphopeptide enrichment and nano LC-MS/MS analyses. Y.M. and Y.O. interpreted the results and wrote the manuscript.

Competing Interests

The authors declare no competing interests.

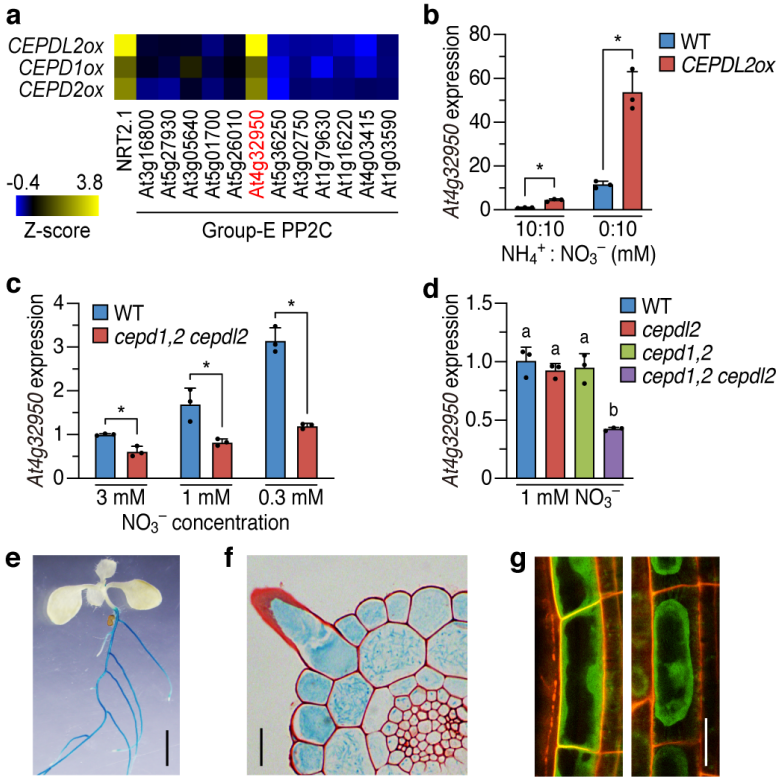

Fig. 1. Overexpression of *CEPDL2/CEPD1/2* induces the expression of *At4g32950* (*CEPH*). (**a**) Expression levels of PP2C-E genes including *At4g32950* in 9-day-old WT plants or transgenic plants overexpressing *CEPDL2*, *CEPD1* or *CEPD2* under N-replete (10 mM NH_4^+, 10 mM NO_3^-) conditions. (**b**) *At4g32950* expression is affected by N composition. (**c**) Expression of *At4g32950* is positively regulated by N starvation through the CEPDL2/CEPD1/2 pathway. (**d**) Expression level of *At4g32950* in *cepdl2* single, *cepd1,2* double and *cepd1,2 cepdl2* triple mutants. (**e**) Histochemical staining of 10-day-old seedlings transformed with the *At4g32950pro:GUS* gene. Scale bar = 2 mm. (**f**) Cross-section of the primary root pictured in (e). Scale bar = 20 µm. (**g**) Subcellular localization of At4g32950-GFP in root epidermal cells before (left) and after (right) plasmolysis, indicating cytosolic localization. Scale bar = 20 µm. Data are presented as the mean ± SD, and each dot represents a biological replicate. For (**b**) and (**c**), statistical significance is determined by two-tailed non-paired Student's *t* test (*P < 0.05). For (**d**), different letters indicate statistically significant differences (P < 0.05, one-way ANOVA with post-hoc Tukey's test). The experiments in (**e**)-(**g**) were repeated twice with similar results.

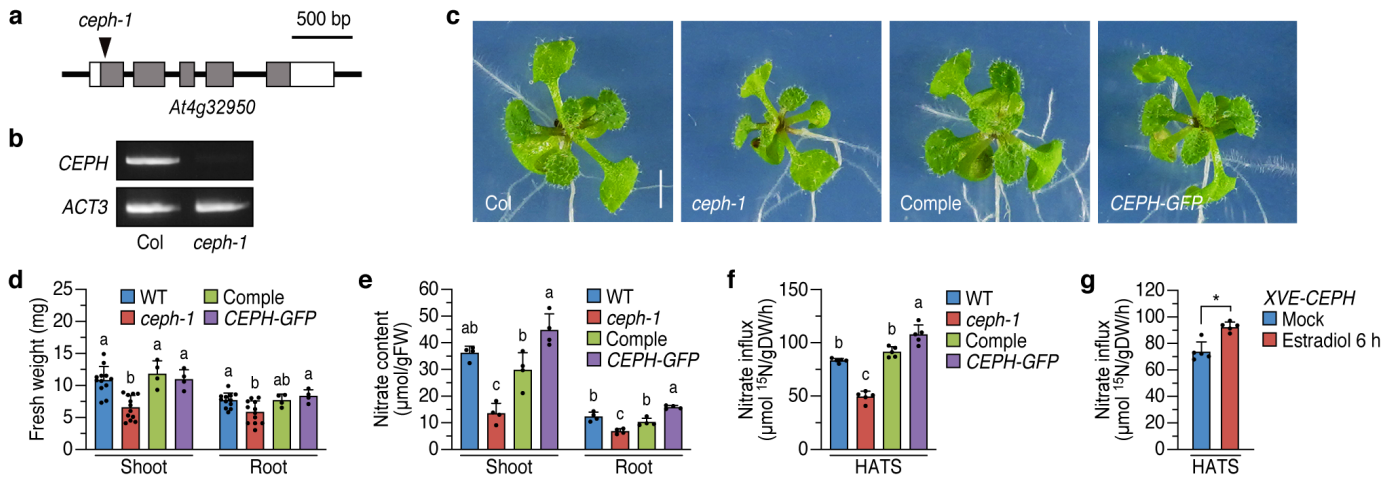

Fig. 2. CEPH positively regulates high-affinity nitrate uptake in roots. (**a**) The T-DNA insertion site of the *ceph-1* mutant in *At4g32950* (*CEPH*). Exons, filled gray rectangles; introns, solid lines; untranslated regions, white rectangles. (**b**) Loss of detectable full-length *CEPH* transcripts in the *ceph-1* mutant, which was verified by RT-PCR. (**c**) Phenotypes of 14-day-old WT, *ceph-1* mutant, and complemented plants grown on 1 mM NO_3^- medium. Scale bar = 2 mm. (**d**) Fresh weight of 14-day-old shoots and roots of WT, *ceph-1* mutant, and *ceph-1* mutant complemented with *CEPH* (T2-2 line) or *CEPH-GFP* (T2-5 line) grown on 1 mM NO_3^- medium. (**e**) Nitrate content in shoots and roots of 14-day-old WT, *ceph-1* mutant, and complemented plants grown on 1 mM NO_3^- medium. (**f**) Root HATS activity of 14-day-old WT, *ceph-1* mutant, and complemented plants grown on 1 mM NO_3^- medium, as determined based on $^{15}NO_3^-$ influx at 0.2 mM. (**g**) Root HATS activity of 14-day-old transgenic *Arabidopsis* plants expressing *CEPH* under control of an estradiol-inducible promoter grown on 10 mM NO_3^- medium. Data are presented as the mean ± SD, and each dot represents a biological replicate. For **(d)-(f)**, different letters indicate statistically significant differences ($P < 0.05$, one-way ANOVA with post-hoc Tukey's test). For (**g**), statistical significance is determined by two-tailed non-paired Student's *t* test (*$P < 0.05$).

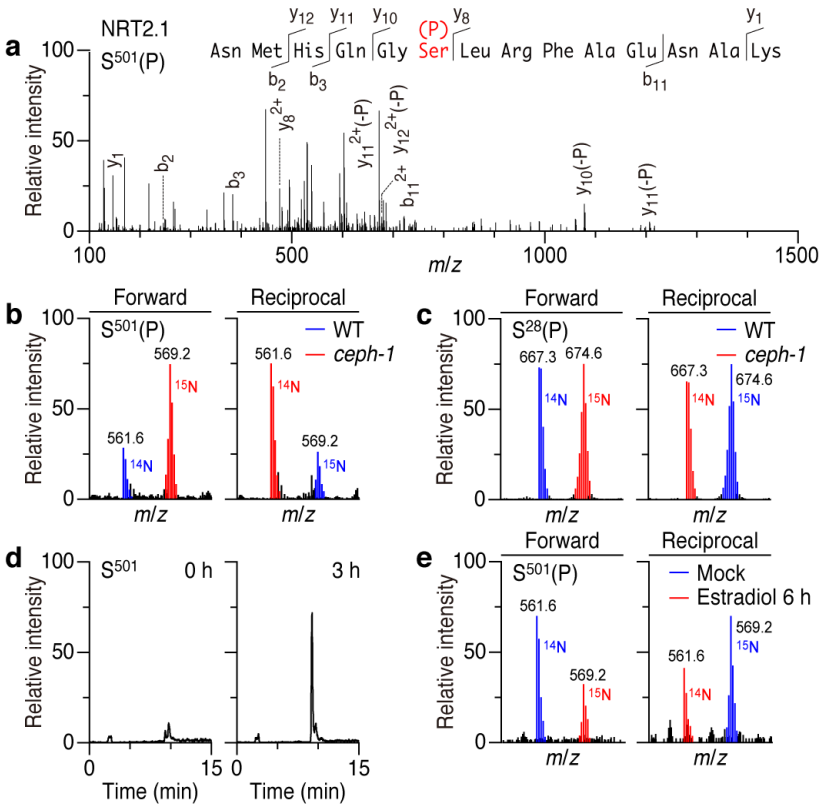

Fig. 3. CEPH directly dephosphorylates S^{501} of NRT2.1. (**a**) MS/MS spectrum of the precursor ion at *m/z* 561.59 corresponding to the triply charged S^{501} phosphopeptide of NRT2.1 (position 496-509 in the NRT2.1 protein sequence), an ion peak specifically increased in *ceph-1*. (**b**) Mass spectra of the NRT2.1 S^{501} phosphopeptide derived from samples of ^{14}N WT/^{15}N *ceph-1* (forward) and ^{15}N WT/^{14}N *ceph-1* (reciprocal) combinations, showing enhanced phosphorylation of the NRT2.1 S^{501} residue in *ceph-1*. (**c**) Mass spectra of the NRT2.1 S^{28} phosphopeptide (position 19-35 in NRT2.1) derived from reciprocally labeled plants, showing comparable phosphorylation levels in WT and *ceph-1*. (**d**) *In vitro* dephosphorylation assay of synthetic 15-residue NRT2.1 S^{501} phosphopeptide with CEPH-GFP. Dephosphorylated peptide was detected by LC-MS in the selected ion monitoring mode at *m/z* 865.9. (**e**) Mass spectra of the NRT2.1 S^{501} phosphopeptide derived from samples of ^{14}N WT/^{15}N *XVE-CEPH* (forward) and ^{15}N WT/^{14}N *XVE-CEPH* (reciprocal) combinations, showing reduced phosphorylation of the NRT2.1 S^{501} residue in *XVE-CEPH* plants after 6 h of estradiol treatment.

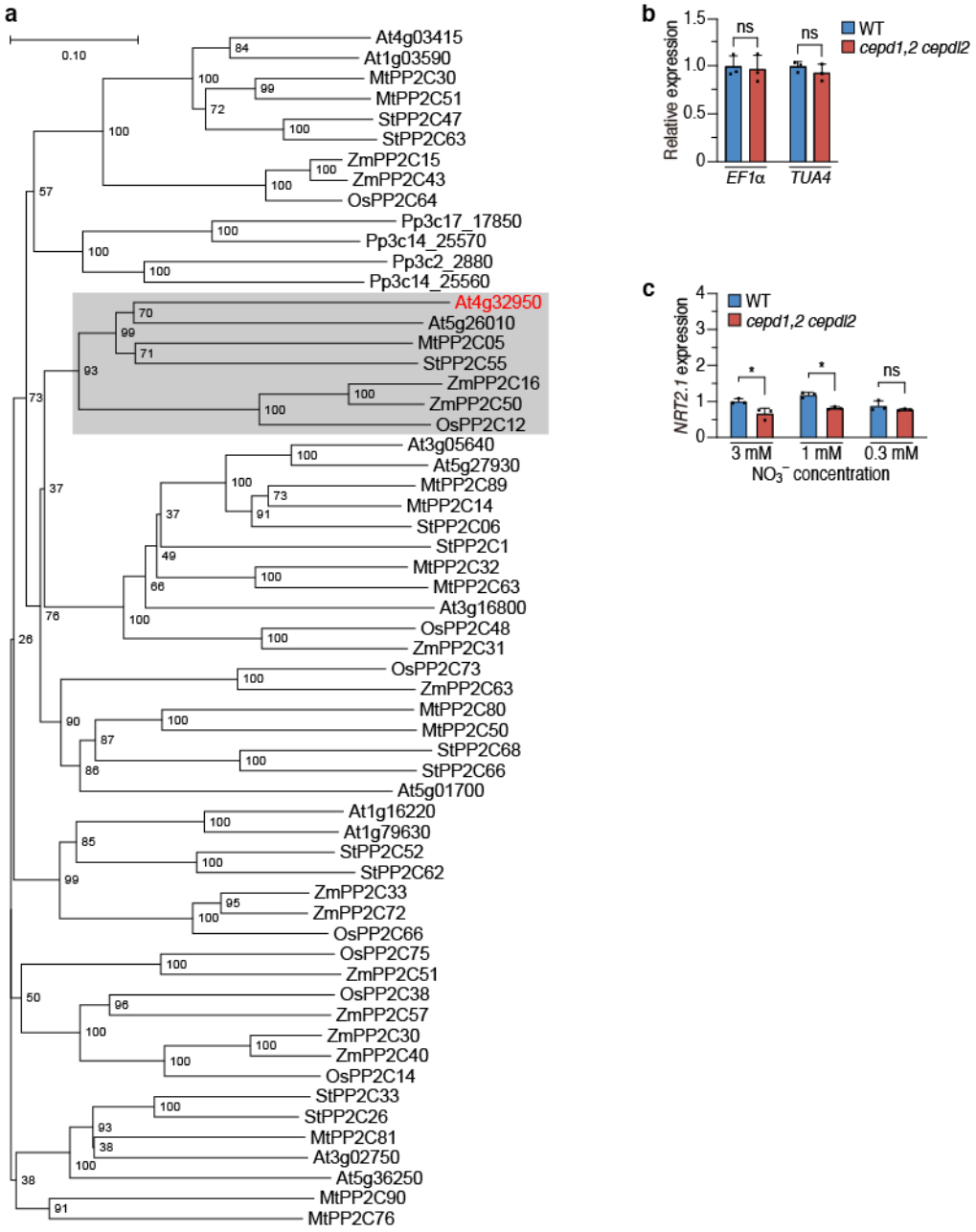

Extended Data Fig. 1. At4g32950 is an *Arabidopsis* PP2C subfamily E protein. (**a**) A combined phylogenetic tree of PP2C subfamily E proteins from *Arabidopsis* (At), potato (St), *Medicago truncatula* (Mt), rice (Os), maize (Zm) and moss *Physcomitrella patens* (Pp). At4g32950 was classified into a distinct clade (shaded) that includes members from potato, *Medicago*, rice and maize, but not mosses. Numbers represent bootstrap values from 1,000 replicates. (**b**) Expression stability of two different reference genes, *EF-1α* and *TUA4*, between WT and *cepd1,2 cepdl2* triple mutant plants. *TUA4* and *EF-1α* expression level in WT and *cepd1,2 cepdl2* was quantified by RT-qPCR using *EF-1α* and *TUA4* as reference genes, respectively. (**c**) Expression of *NRT2.1* in WT and *cepd1,2 cepdl2* triple mutant plants. Data are presented as the mean ± SD, and each dot represents a biological replicate. For (**b**) and (**c**), statistical significance is determined by two-tailed non-paired Student's *t* test (*P < 0.05).

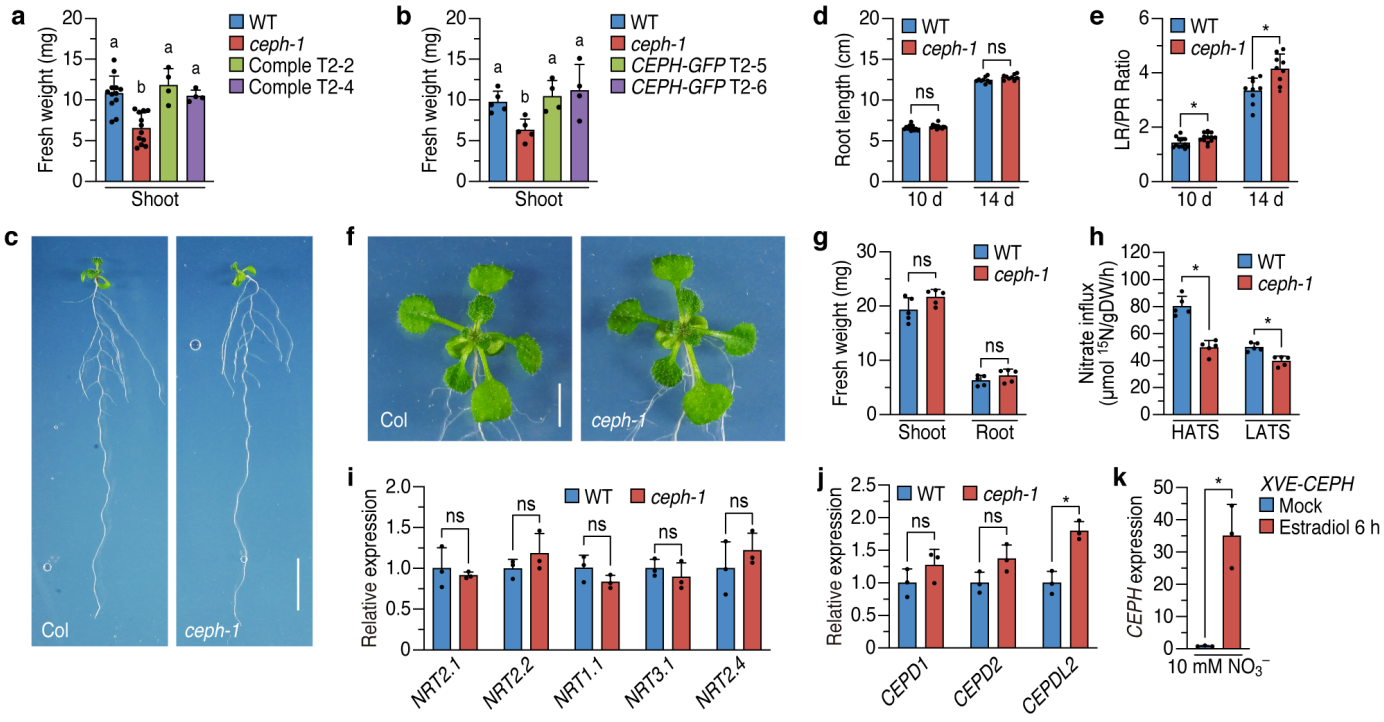

Extended Data Fig. 2. Phenotypic analysis of *ceph-1* mutant plants. (**a**) Fresh weight of 14-day-old shoots of WT, *ceph-1* mutant, and *ceph-1* plants complemented with *CEPH* grown on 1 mM NO_3^- medium. (**b**) Fresh weight of 14-day-old shoots of WT, *ceph-1* mutant, and *ceph-1* plants complemented with *CEPH-GFP* grown on 1 mM NO_3^- medium. (**c**) Root phenotypes of 10-day-old WT and *ceph-1* mutant plants grown on 1 mM NO_3^- medium. Scale bar = 1 cm. (**d**) Primary root length of 10- or 14-day-old WT and *ceph-1* mutant plants grown on 1 mM NO_3^- medium. (**e**) Ratio of total lateral root (LR) length to primary root (PR) length of 10- or 14-day-old WT and *ceph-1* mutant plants grown on 1 mM NO_3^- medium. (**f**) Phenotypes of 14-day-old WT and *ceph-1* mutant plants grown under N-replete conditions (10 mM NH_4^+, 10 mM NO_3^-). Scale bar = 5 mm. (**g**) Fresh weight of the shoots and roots described in (f). (**h**) HATS and calculated LATS NO_3^- uptake activities of 14-day-old WT and *ceph-1* mutant plants grown on 1 mM NO_3^- medium. (**i**) Expression of nitrate transporter genes in WT and *ceph-1* mutant plants. (**j**) Expression of *CEPD1/2* and *CEPDL2* in WT and *ceph-1* mutant plants. (**k**) Induction level of *CEPH* in *XVE-CEPH* plants 6 h after estradiol treatment. Data are presented as the mean ± SD, and each dot represents a biological replicate. For (**a**) and (**b**), different letters indicate statistically significant differences ($P < 0.05$, one-way ANOVA with post-hoc Tukey's test). For (**d**), (**e**) and (**g**)-(**k**), statistical significance is determined by two-tailed non-paired Student's *t* test (*$P < 0.05$).

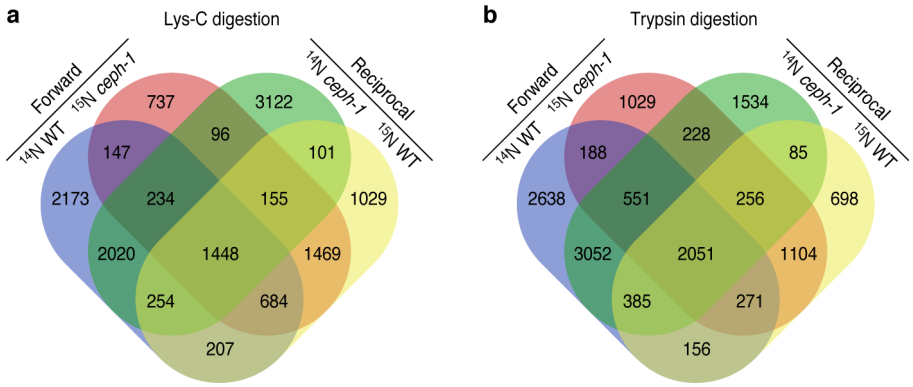

Extended Data Fig. 3. Venn diagram showing overlap between data sets. (**a**) Venn diagram for numbers of phosphopeptide ion peaks identified in the Lys-C–digested samples and overlap between the forward and reciprocal analyses. (**b**) Venn diagram for numbers of phosphopeptide ion peaks identified in the trypsin-digested samples and overlap between the forward and reciprocal analyses.

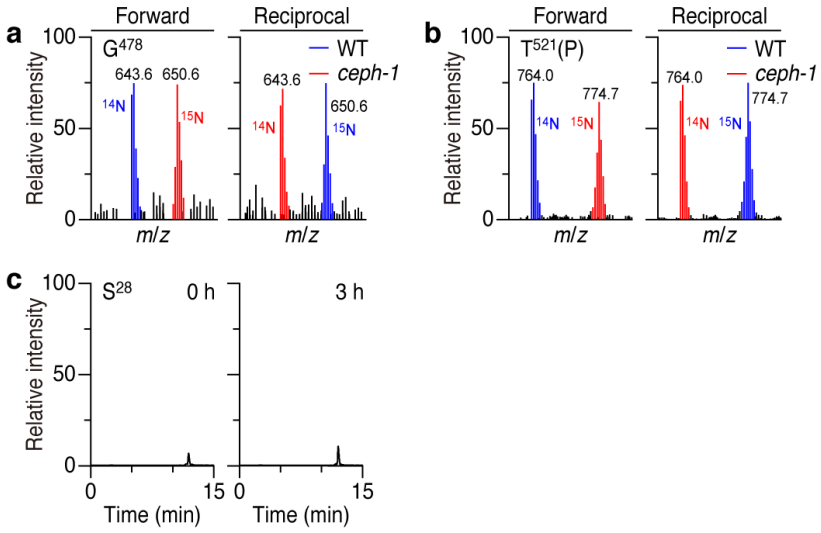

Extended Data Fig. 4. Quantitative phosphoproteomic analysis of the CEPH substrate. (**a**) Mass spectra of the NRT2.1 G^{478} nonphosphorylated peptide (position 478-493 in NRT2.1 protein) derived from reciprocally ^{14}N- and ^{15}N-labeled plants, showing comparable NRT2.1 protein abundance in WT and *ceph-1* plants. (**b**) Mass spectra of the NRT2.1 T^{521} phosphopeptide (position 516-530 in NRT2.1) derived from reciprocally labeled plants, showing comparable phosphorylation levels in WT and *ceph-1* plants. (**c**) Dephosphorylation of the NRT2.1 S^{28} phosphopeptide with CEPH-GFP detected by LC-MS in the selected ion monitoring mode at *m*/*z* 831.9.

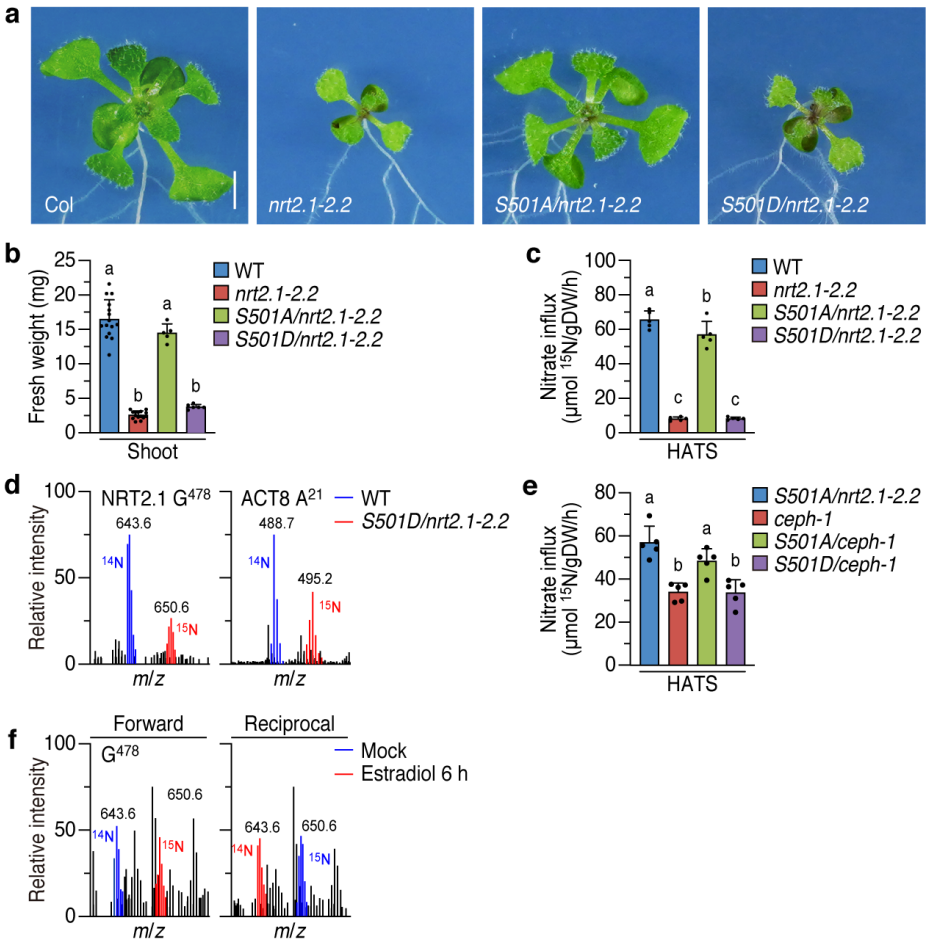

Extended Data Fig. 5. NRT2.1 S^{501} phosphorylation acts as a negative phospho-switch that represses HATS activity. (**a**) Phenotypes of 14-day-old WT, *nrt2.1-2.2* mutant, *nrt2.1-2.2* complemented with *NRT2.1[S501A]* and *nrt2.1-2.2* complemented with *NRT2.1[S501D]* grown on 1 mM NO_3^- medium. Scale bar = 2 mm. (**b**) Fresh weight of 14-day-old shoots of the plants shown in (a). (**c**) Root HATS activity of the plants shown in (a). (**d**) Mass spectra of the NRT2.1 G^{478} nonphosphorylated peptide (position 478-493 in NRT2.1 protein) and ACT8 A^{21} peptide (position 21-30 in ACT8 protein) derived from WT and NRT2.1[S501D] plants. Decrease in ACT8 protein abundance in S501D plants suggests the decrease in overall protein expression level is due to a nitrate uptake defect in S501D plants. Considering this, protein abundance of NRT2.1 was not significantly affected by the S501D mutation. (**e**) Root HATS activity of 14-day-old *nrt2.1-2.2* mutant plants complemented with *NRT2.1[S501A]*, *ceph-1* mutant, *ceph-1* mutant expressing *NRT2.1[S501A]* and *ceph-1* mutant expressing *NRT2.1[S501D]*. The plotted *S501A/nrt2.1-2.2* data is the same as that shown in Extended Data Fig. 5c, as the experiments were done concurrently. (**f**) Mass spectra of the NRT2.1 G^{478} nonphosphorylated peptide (position 478-493 in NRT2.1 protein) derived from reciprocally ^{14}N- and ^{15}N-labeled plants, showing comparable NRT2.1 protein abundance in mock and estradiol-treated *XVE-CEPH* plants. Data are presented as the mean ± SD, and each dot represents a biological replicate. For (**b**), (**c**) and (**e**), different letters indicate statistically significant differences ($P < 0.05$, one-way ANOVA with post-hoc Tukey's test).

Supplementary Table 1. List of the top 10 CEPDL2/CEPD1/2-regulated genes in roots. Table includes the GeneChip signal intensity, signal intensity ratio (Log_2FC), Z-score, and gene description. Results are sorted by the Z-score of *CEPDL2ox* plants.